Shape Memory Alloy (SMA) Damping for Smart Miniature Systems

Kiran Jacob, Shahabeddin Ahmadi, Pejman Shayanfard, Frank Wendler, and Manfred Kohl

1 Introduction

In many applications, uncontrolled mechanical vibrations are a potential source of noise and damage. On the large scale, dampers are used in massive structures like buildings and bridges to reduce the impact of seismic loads, or in automobiles, to improve travel comfort and safety [1]. In the past couple of decades, there is a strong drive towards miniaturization with integration of many sensors/actuators at small footprint [2]. Vibration damping and control for small and micro-scale systems is challenging, as most damper concepts used for large structures cannot easily be downscaled. Here, the authors develop miniature dampers and vibration control using Shape Memory Alloy (SMA) foil based devices for miniature robotics application and smartphone camera stabilization against hand movements. By using SMA foils, design flexibility and miniaturization are achieved.

SMAs are functional materials capable of undergoing large reversible deformation through which a lot of energy is dissipated. This unique behaviour is attributed to the underlying phase transformation of the material between austenite and martensite phases. Unlike many other velocity dependent damper concepts, the energy dissipation in SMA is heavily dependent on the loading strain. SMAs exhibit two types of behaviours called pseudoelasticity or one-way shape memory effect depending on the operating temperature. The material shows pseudoelasticity when operated above austenite finish temperature (A_f) and one-way shape memory effect below marten-

---

K. Jacob · S. Ahmadi · M. Kohl (✉)
Institute of Microstructure Technology, Karlsruhe Institute of Technology,
Hermann-von-Helmholtz-Platz 1, 76344 Eggenstein-Leopoldshafen, Germany
e-mail: manfred.kohl@kit.edu

P. Shayanfard · F. Wendler
Friedrich-Alexander-Universität Erlangen-Nürnberg, Institute of Materials Simulation,
Dr.-Mack-Str. 77, 90762, Furth, Germany
e-mail: frank.wendler@fau.de

P. Eberhard (ed.), *Calm, Smooth and Smart*, Lecture Notes in Applied
and Computational Mechanics 102, https://doi.org/10.1007/978-3-031-36143-2_7

site finish temperature (M_f). In pseudoelastic SMA, the strain recovery occurs upon unloading. In a mechanical loading cycle, large amount of energy is dissipated by material hysteresis which is used to develop passive dampers. In one-way SMA, the strain recovery occurs when the material is heated above A_f. This principle is used to develop active dampers and actuators for vibration control.

This article is structured as follows: in Sect. 2 the pseudoelastic material behaviour and passive damper performance under shock loading are illustrated. In Sect. 3, concepts for active damping based on the one-way SMA effect are introduced, and a related multi-axial constitutive model is sketched. In Sect. 4, a 2-DoF vibration stabilization platform using one-way SMA actuators is described.

2 Damping Using Pseudoelastic SMA Devices

A cold-rolled $Ni_{50.5}Ti_{49.1}Fe_{0.4}$ (at. %) foil of 30 μm thickness is used to investigate the passive damping behaviour of SMA. This material shows pseudoelastic behaviour at room temperature. The stress-induced transformation between austenite and martensite is responsible for the energy dissipation in pseudoelastic SMA. In this section, the behaviour of the material, damper devices and passive damper systems is described.

2.1 Material Behaviour

The mechanical behaviour of pseudoelastic SMA is investigated by displacement-controlled uniaxial tensile loading of a strip of SMA foil having dimensions (l, w, t): 10, 3, 0.03 mm. Figure 1a shows the tensile loading at various loading strains. Above a critical stress of about 500 MPa, the phase transformation to martensite is initiated resulting in the plateau region in stress-strain behaviour. A large strain of 0.04 is accommodated during the transformation to martensite. The material recovers to its initial state upon unloading. A large amount of loading energy is dissipated via hysteresis in this cyclic operation. The energy dissipation increases with increase in loading strain. Figure 1b illustrates the effect of pre-straining (ε_{pre}) on energy dissipation while retaining a constant loading strain of 0.01 with reference to the loading behaviour at zero pre-strain. The material has a non-linear behaviour with an initial elastic region until about 0.02 strain where the material remains in austenite and thereafter a plateau region where the transformation to martensite occurs. At pre-strain of 0.01 ($\varepsilon_{\text{pre1}}$) and loading strain of 0.01, not much energy dissipation is observed owing to predominant elastic behaviour. Adjusting the pre-strain close to the beginning of transformation plateau at 0.02 ($\varepsilon_{\text{pre2}}$), an almost repeatable energy dissipation is observed for loading cycles. Fixing the pre-strain in the elastic region enables the material to completely recover to its starting condition. Further increase in pre-strain to 0.03 ($\varepsilon_{\text{pre3}}$), high energy dissipation in the first loading cycle is attained

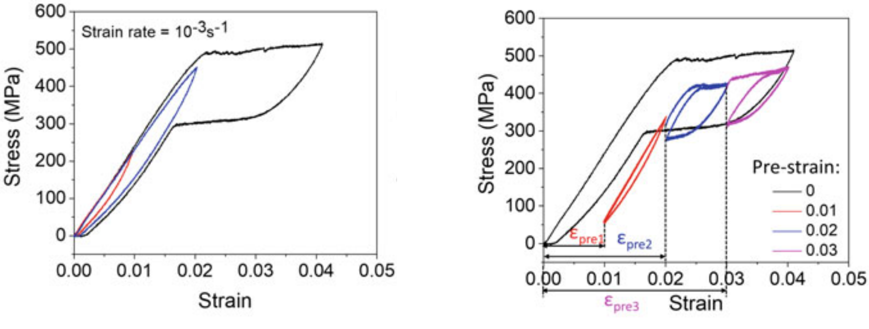

(a) (b)

Fig. 1 Material hysteresis behaviour under uniaxial tensile loading for various loading strains (**a**) and at fixed loading strain of 0.01 (**b**)

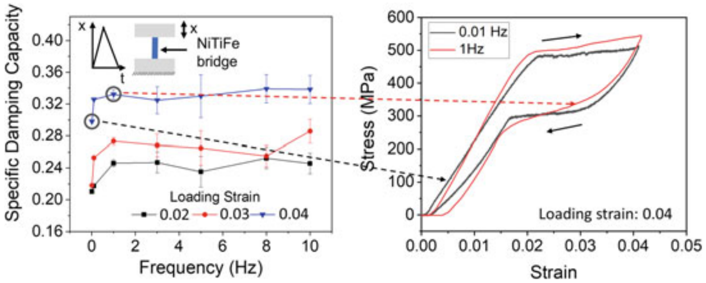

Fig. 2 SDC behaviour at various frequencies and loading strains showing increase in hysteresis until adiabatic loading is reached above 1 Hz

but subsequent cycles show reduced energy dissipation. Therefore, pre-strain and loading strain are crucial parameters for optimizing dissipation.

The energy dissipation of the material at various frequencies and loading strains is shown in Fig. 2. The energy dissipation arising from the material hysteresis is quantified using the parameter called Specific Damping Capacity ($\mathrm{SDC}_{\mathrm{material}}$), which is the ratio of energy dissipation through hysteresis to the loading energy. Until loading frequencies upto 1 Hz there is an increase in $\mathrm{SDC}_{\mathrm{material}}$ due to increase in hysteresis. This effect is associated with the self-heating of the material during the transformation to martensite. Owing to this temperature rise in the material, an increase in loading stress is required for transformation. Above 1 Hz, adiabatic heating is attained, resulting in a frequency independent $\mathrm{SDC}_{\mathrm{material}}$ behaviour.

2.2 Double Bridge Device and Passive Damper System

Designing of the damper device is based on the load to be supported and the external excitation. A passive damper device with double bridge structure is micromachined by laser cutting from SMA foil as shown at the top of Fig. 3 (drawing not to scale). The half-bridge dimensions of the device are $5 \times 0.3 \times 0.03$ mm^3 (L_0 w, t). The device is designed to operate in out-of-plane direction. The bridges of the device are strained to 0.05 for an out-of-plane loading displacement of 1.6 mm. The pre-strain of the device is adjusted along the in-plane direction.

The damper system is constructed from two double bridge devices sandwiching a mass of 18 g as shown in Fig. 3. The mass is pulled using an electromagnet and released by deactivating the electromagnet. The free oscillation of the mass is tracked using a laser displacement sensor. The SDC for the system is evaluated for the first oscillating cycle as

$$SDC_{system} = 1 - \left(\frac{x_1}{x_{max}}\right)^2, \tag{1}$$

where x_{max} is the shock loading amplitude and x_1 is the first peak of free oscillation. SDC$_{\text{system}}$ is higher than the SDC$_{\text{material}}$ described in Sect. 2.1 owing to the presence of air drag and structural damping in the system. Figure 4 shows the SDC$_{\text{system}}$ at various loading amplitudes and pre-strains for the first oscillation cycle. SDC$_{\text{system}}$ increases with increase in loading amplitude and pre-strain. This trend continues until the combined strain due to pre-strain and loading strain is not exceeding complete martensite transformation strain of 0.05. Therefore, for a particular loading amplitude, pre-strain optimization enables improved energy dissipation. Maximum SDC$_{\text{system}}$ of 70 % is reached utilizing maximal material hysteresis for energy dissipation, implying that only 30 % of the loading energy is remaining. After the first oscillation cycle, the mass undergoes several low amplitude oscillations before reaching equilibrium position. Owing to the lack of guidance for the mass, various modes of oscillations are observed in this settling behaviour.

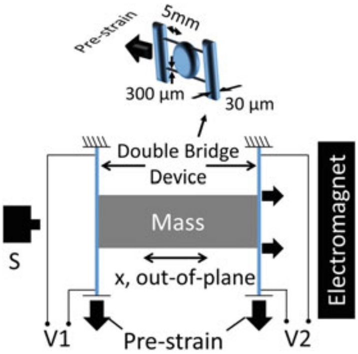

Fig. 3 The schematic of damper test setup [3] and an image of the double bridge device is shown at the top (drawing not to scale). Legends: S-Displacement sensor, V1,V2-Terminals for heating pulse (used while using one-way devices)

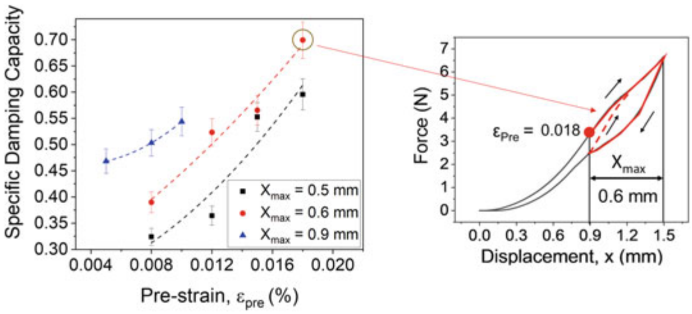

Fig. 4 SDC behaviour of pseudoelastic damper system at various pre-strains and shock loading amplitudes

2.3 Single Bridge SMA Device and Passive Damper System

A prospective application of the SMA damper is the shock absorption in miniature robotics, where vertical shock loads are of interest. As illustrated in Sect. 2.2, high energy dissipation is achieved under shock loading. The lack of mass guidance resulted in 3D mass movement after release from the electromagnet. In this section, the behaviour of SMA shock absorber under vertical shock loading with guided mass movement is illustrated.

A single bridge damper device design is used as the mass is balanced using the guidance. The bridge has a dimension of w= 1 mm and L_0= 6 mm, allowing for an out-of-plane displacement of 1.9 mm at a strain of 0.05 in the bridge.

The test setup for the shock absorber is illustrated in Fig. 5. A mass of 47 g is connected to the damper device and its movement is guided using a low friction linear bearing. The shock loading is provided using an electromagnet. The movement of the mass is tracked using a laser displacement sensor. Data acquisition and control system is used to acquire the measurement and to control the electromagnet.

Fig. 5 Schematic of test setup for vertical shock loading

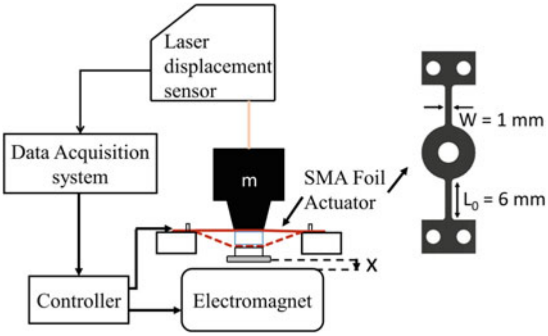

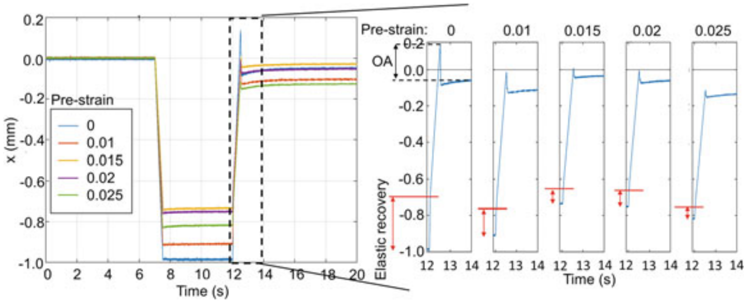

Fig. 6 The shock response of the system at various device pre-stains and the zoomed in settling behaviour showing an increase in overshoot amplitude with increase in elastic recovery

The shock response of this device under various pre-strains is shown in Fig. 6. The shock loading amplitude is selected to limit the total created strain on the SMA device to 0.045. In all loading experiments, the mass stabilizes immediately after the first overshoot demonstrating excellent shock damping performance. A closer look on the settling behaviour reveals the contributions of elastic recovery and material hysteresis. Elastic recovery, resulting in a sudden mass movement, occurs immediately after release as marked by the red lines. Apparently, the elastic recovery changes with the pre-strain and loading conditions. Accordingly, the overshoot amplitude (OA) follows the same trend as elastic recovery showing high OA at high elastic recovery. This study reveals the effectiveness of using SMA foil based passive damper as miniature shock absorber.

2.4 *Development of a FEM Model for Pseudoelastic Damping*

The mechanical response of SMAs is both nonlinear and history dependent due to a first order structural phase transition from austenite (A) to martensite (M), which is related to the release (A → M) or the uptake (M → A) of latent heat. The strong thermomechanical coupling requires transient, time-resolved simulations as the deformation depends on the history of the internal state variables. The local character of the transition observed in experiments necessitates a spatially resolved, mesoscale description of the sample geometry, for which the authors use a finite element approach.

2.4.1 SMA Constitutive Material Model

Taking the original 1D approach from Müller et al. [4] as a basis, a plane-stress 2D constitutive model for tensile loaded thin films was developed in [5]. The model is based on a thermodynamic description using a Gibbs free energy density

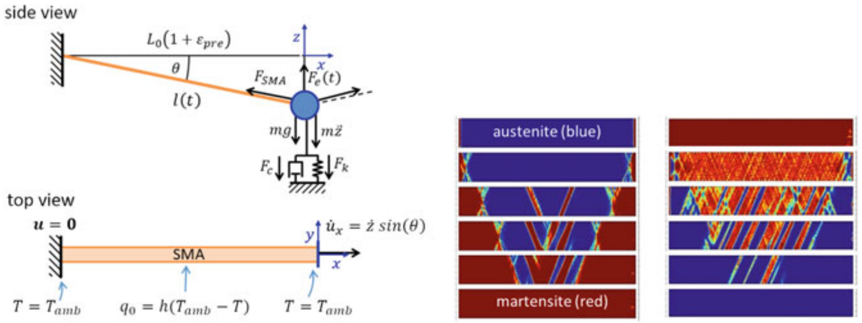

(a) (b)

Fig. 7 (**a**) Force balance assumed in the ODE for mass displacement z (top) and 2D FE domain with boundary conditions (bottom) [6]. (**b**) Top → bottom: time evolution of martensite fraction in SMA bridge during loading (left) and unloading (right), at equidistant time steps of 10 s

$$g(\varepsilon, \sigma, T, x_\alpha, \nabla x_\alpha) = \Psi_{mech}(\sigma, \varepsilon) - \sigma\varepsilon + \Psi_{chem}(T) + \Psi_{PF}(x_\alpha, \nabla x_\alpha),$$

that depends on local values of strain ε, stress σ, temperature T, the fraction of phases x_α, and their gradients ∇x_α. The existence of tension and compression accommodated martensite variants ($\alpha = M_+, M_-$) and austenite ($\alpha = A$) is assumed. Twinned martensite is represented as 50–50 mixture of M_+ and M_-. The mechanical part of the free energy Ψ_{mech} forms a non-convex continuous three-well potential in linear strain space, whereas the chemical part Ψ_{chem} controls the energy difference between austenite and martensite phase. A phase-field energy term Ψ_{PF} for a coarse-grained treatment of A-M interface energies was incorporated [5, 7]. Rate equations for the phase fractions X_{M_-}, X_A and X_{M_+} are formulated as

$$\begin{aligned}
\dot{x}_{M_+} &= -x_{M_+} p^{x_{M_+}A} + x_A p^{Ax_{M_+}} - \frac{\omega}{W}\delta\Psi_{PF}/\delta x_{M_+}\\
\dot{x}_{M_-} &= -x_{M_-} p^{x_{M_-}A} + x_A p^{Ax_{M_-}} - \frac{\omega}{W}\delta\Psi_{PF}/\delta x_{M_-}\\
\dot{x}_A &= -\dot{x}_{M_+} - \dot{x}_{M_-},
\end{aligned}$$

where $\delta/\delta x_{M_\pm}$ denotes a variational derivative. By this approach the authors assume thermally activated kinetics describing transitions from compression-accommodated M_- over austenite A to tension-accommodated martensite M_+, where stress and temperature dependent transition rates $p^{\alpha\beta}(\sigma - \sigma^{\alpha\beta}, T)$ are used. The plateau stresses $\sigma^{\alpha\beta} = (\sigma_0^{\alpha\beta} + C^{\alpha\beta}(T - T_R))(1 + \xi)$ define the transformation criteria [5]. Here, a static noise field for the transformation stress level ξ is introduced to capture heterogeneous nucleation sites not observable on the device level. In this way, in simulations, local deformation pattern like Lüders-like bands are developing, where the properties of the noise distribution ξ are adjusted in comparison with DIC (digital image correlation) images from experiment.

2.4.2 FEM Setup for Simulating Bridge Vibrations

Due to the low thickness of the SMA films of a few tens of microns, bending deformation of the bridge dampers can be neglected, as the related stresses amount for only a few percent of those created by the tensile stretch. This was also verified by a good match between measured quasi-stationary force-displacement curves and calculated ones, where the stress-strain characteristics of the material was used. For transient simulations of pseudoelastic single bridges, the setup including mechanical and thermal boundary conditions is shown in Fig. 7a. The SMA domain is discretized with high spatial resolution in the FE model assuming 2D plane stress conditions (top view), whereas the equation of motion of the attached mass is given as the force balance (side view) of the proof mass, resulting in

$$m\ddot{z} - mg + 2F_{SMA}(t)sin(\theta) - F_e(t) = 0 \quad \text{with} \quad sin(\theta) = \frac{z}{\sqrt{z^2 + l_0^2(1+\varepsilon_{pre})^2}},$$

where l_0 denotes initial SMA length and ε_{pre} the applied pre-strain. This one-DoF ODE is solved simultaneously, where the coupling of mass position z and displacement, u, at the FE domain boundary is achieved by a boundary condition for the longitudinal displacement rate $\dot{u}_x = \dot{z}sin(\theta)$ assuming a stretched geometry with angle θ. For a quasi-stationary displacement of the mass in z-direction (Fig. 7a), the time evolution of the martensite fraction due to the occurring tensile load is shown in Fig. 7b.

The transient mass amplitude and martensite fractions are given in Fig. 8a for a single bridge device excited with a harmonic force of 0.1 N and 32 Hz. Simulations were conducted with the parameter set in Table 1 determined from characterization data of the quarternary alloy NiTiCoCu. Both curves show the evolution of a steady state after an initial settling phase. For operation of the devices close to the resonance

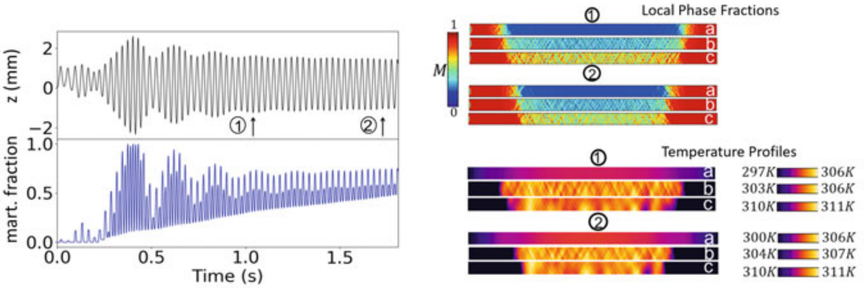

(a) (b)

Fig. 8 (**a**) Time data of mass displacement z and martensite fraction x_{M_+} for a harmonically loaded single bridge device (32 Hz, 0.1 N, m =10 g); (**b**) local patterns of martensite fraction and temperature, at the two time steps indicated in (**a**) [8]

Table 1 Simulation parameters for a pseudoelastic NiTiCuCo damper device [7] and a one-way TiNi device [6]

Parameter	Symbol	Pseudoelastic SMA	One-way SMA
Proof mass	m	0.01 kg	0.018 kg
Length/width/thickness, SMA	$l/w/d$	10/0.35/0.02 mm	5/0.3/0.03 mm
Plateau stress A-M	σ^{AM}	242 MPa	495 MPa
Plateau stress M-A	σ^{MA}	134 MPa	100 MPa
Reference temp. for σ^{AM}/σ^{MA}	T_{ref}	294 K	349.7 K
Clausius-Clapeyron coeff. A-M	C^{AM}	10.4 MPa K^{-1}	5.8 MPa K^{-1}
Clausius-Clapeyron coeff. M-A	C^{MA}	14 MPa K^{-1}	6.2 MPa K^{-1}
Transformation strain	ε_T	0.0075	0.04
Elastic modulus, A	E_A	35.9 GPa	70.2 GPa
Elastic modulus, M	E_M	16.0 GPa	32.2 GPa
Latent heat	L	5600 J kg^{-1}	22130 J kg^{-1}
Thermal conductivity, A	k_A	18 $Wm^{-1}K^{-1}$	18 $Wm^{-1}K^{-1}$
Thermal conductivity, M	k_M	8.6 $Wm^{-1}K^{-1}$	8.6 $Wm^{-1}K^{-1}$
Heat transfer coefficient	h	30 Wm^{-2} K^{-1}	30 Wm^{-2} K^{-1}

of the bridge oscillator, generally a continuous accumulation of martensite is found, hence a steady decay of damping capacity follows. Representative local fine-banded patterns of phase fraction and temperature are given in Fig. 8b, which shows that martensite accumulation proceeds from the fixed boundaries of the SMA.

3 Damping Using One-Way SMA Devices

So far, the passive damping of SMA devices exploiting stress induced phase transformation is explained. By using SMA devices showing one-way shape memory effect, heating pulses can be utilized to stimulate phase transformation allowing for an external control of the energy dissipation. To investigate the active damping behaviour of SMA, cold-rolled NiTi foil of 30 μm thickness is used here. This material shows one-way effect at room temperature, retaining its strain upon loading owing to the reorientation of martensite. Strain recovery occurs by heating the material above austenite finish temperature to enable phase transformation to austenite. A large part of the loading energy is dissipated in this cyclic operation. In this section, the damping behaviour of one-way material based damper devices and damper systems is described [3, 9].

3.1 Material Behaviour

The phase transformation behaviour of a $Ti_{50.2}Ni_{49.8}$ (at. %) foil measured using Differential Scanning Calorimetry (DSC) is shown in Fig. 9a. The material transforms to austenite at temperatures above the austenite finish temperature A_f. When cooling down, the material transforms to martensite via an intermediate R-phase. However, macroscopically, the effect of R-phase is observed as a small plateau only in the first loading cycle near to a loading strain of 0.005 . Therefore the phase of the material below the R finish temperature (R_f) of 43.2 °C is referred to as the starting phase in this article.

A strip of one-way SMA foil having dimension $10\times3\times0.03\,\text{mm}^3$ is uniaxially loaded in displacement controlled mode to a loading strain of 0.04 at various frequencies in a thermal chamber, the corresponding SDC, estimated from the material hysteresis as explained in Sect. 2.1, is shown in Fig. 9b. The maximum SDC is achieved for loading at 25 °C. The SDC of the material decreases significantly with increase in temperature. At 60 °C, the material is in austenite and exhibits pseudoelastic behaviour demonstrating a lower SDC of about 45 %.

The damping capacity of the material at various loading strains and frequencies is shown in Fig. 10. The $\text{SDC}_{\text{material}}$ increases with increasing loading amplitude and attains a maximum of 86 % under quasi-stationary loading conditions. Also, the $\text{SDC}_{\text{material}}$ shows a reduction with frequency up to 1 Hz, which is caused by the increase in transformation stress arising from the self-heating of the material. The self-heating raises the material temperature above A_s resulting in enhanced elastic recovery. After reaching an adiabatic loading situation at 1 Hz, the $\text{SDC}_{\text{material}}$ shows a nearly frequency independent behaviour.

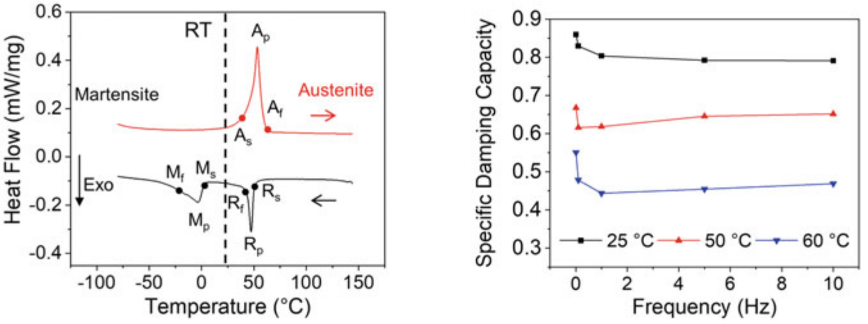

(a) (b)

Fig. 9 The phase transformation behaviour of one-way SMA (**a**) and its temperature dependent SDC behaviour at various ambient temperatures (**b**). Legends: Austenite–$A_{s,p,f}$: 47.2, 54.2, 59.1 °C, R-phase–$R_{s,p,f}$: 50.3, 47.9, 43.2 °C, Martensite–$M_{s,p,f}$: 2.0, –5.1, –28.5 °C (temperatures listed as start, peak, finish)

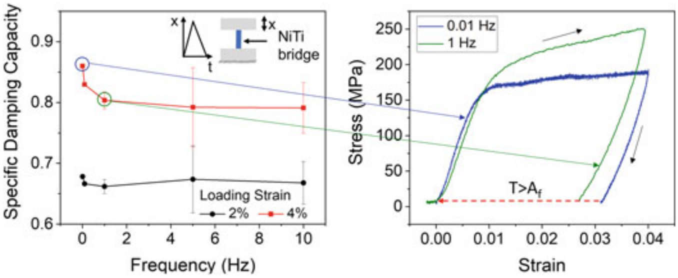

Fig. 10 SDC behaviour of one-way SMA strip under tensile testing showing reduction in damping capacity until reaching the adiabatic loading condition at 1 Hz

3.2 Double Bridge Device and Active Damper System

The double bridge device design explained in Sect. 2.2 is also used to develop one-way SMA devices to investigate their active damping performance. For active damping, the phase transformation to austenite is attained by electrical heating pulses. The pulse duration of 50 ms is chosen to enable the transformation within the first cycle of free oscillation, and leads to an inhomogeneous temperature distribution along the bridges.

The maximum temperature in the device (T_{max}) is shown in Fig. 11. The device heats-up from the initial room temperature to 80 °C when a heating pulse of 1 W is applied for 50 ms. Under this condition, more than 90 % of the bridge is at a temperature above A_f. The time to cool down to 90 % of the maximum bridge temperature lies between 1.2 and 1.3 s. This large cooling time limits the effectiveness of applying multiple heating pulses during free oscillation after shock loading.

The test setup explained in Sect. 2.2 is used to investigate the active shock damping performance. Terminals V1 and V2 in Fig. 3 are used to apply the heating pulses to enable phase transformation to austenite. Figure 12 shows the SDC_{system} at various pre-strains and shock loading amplitudes for this one-way damper system. The heating pulse is applied when the mass moves 0.3 mm after the release from the electromagnet. The SDC measurement for the first oscillation cycle shows an increase

Fig. 11 The maximum temperature on the double bridge device for various heating pulses of 50 ms duration, and related time to cool-down to 90 % of the raised temperature

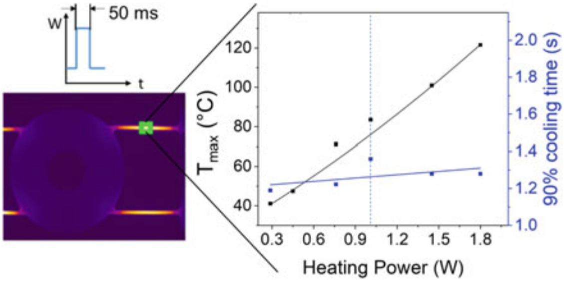

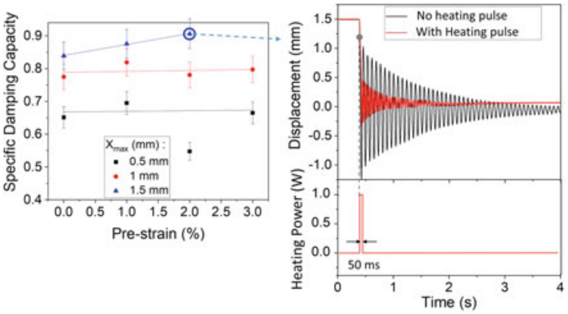

Fig. 12 SDC of double bridge active damper system depending on pre-strain and amplitude (left), and comparison of active and passive modes of operation (right) for a pre-strain of 2.0 % and a loading amplitude of 1.5 mm [9]

with the increase in loading amplitude and reaches a maximum of about 90 % resulting in a large reduction in oscillation amplitudes and settling time.

3.3 Single Bridge Device and Active Damper System

As for the pseudoelastic passive damper system in Sect. 2.3, the motion constrained to a single DoF is investigated for the one-way SMA device under vertical shock loading.

The thermal behaviour of the device after pulse and continuous heating is investigated to optimize the thermally-induced phase transition. Figure 13 shows the temperature distribution along a half-bridge. An improved homogeneity of the temperature distribution is achieved at a short heating pulse of 0.89 W for 100 ms indicating adiabatic conditions for the device below 100 ms. After the heating pulse, the cooling down time to reach the starting phase is about 0.75–1 s.

For the single DoF device, a short current pulse of 75 ms is applied on the SMA device at the instance of the electromagnet being turned OFF. A systematic study of the response for various mass and pre-strains is conducted (Fig. 14). The shock loading amplitude of the different pre-strains depicted in Fig. 14b is chosen to limit the total strain in the SMA to 0.045 to avoid overloading. The total strain is composed of pre-strain, loading strain of the device due to the supported mass, and strain introduced by the shock loading. Under test conditions of varying mass and pre-strains, the system shows a similar relaxation, indicating that this settling behaviour is determined by the phase transformation of the material alone. After the removal of heating pulse, a small overshoot of the mass displacement is visible. This arises due to the strong recovery force that persists until the temperature falls below R_f, resulting in the overshoot. Thereafter, the SMA device gradually relaxes to equilibrium. At all these examined loading conditions, oscillation-free fast settling is demonstrated by this damper system.

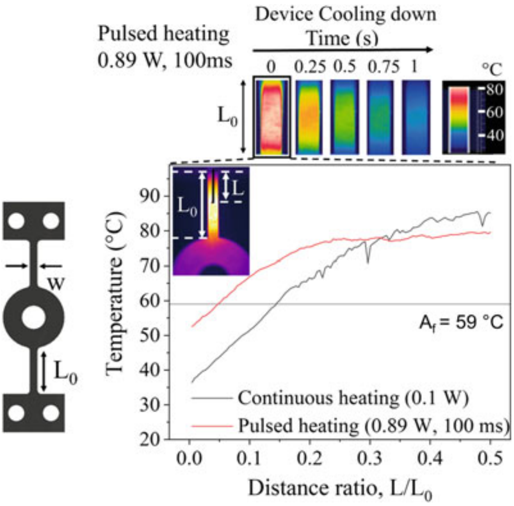

Fig. 13 Thermal distribution along the bridges with the application of continuous and pulsed heating [10]

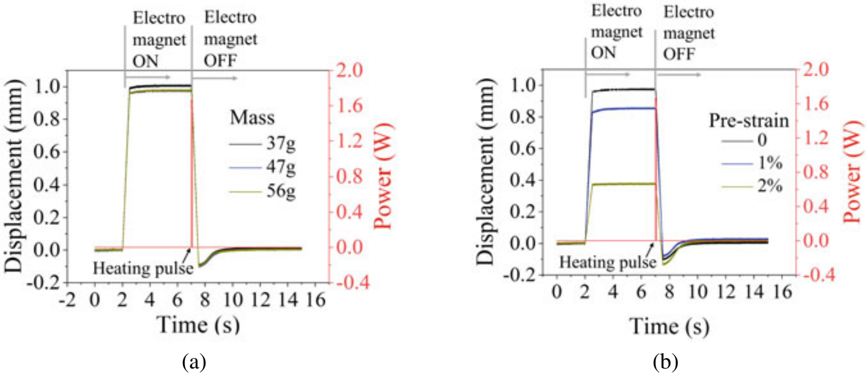

Fig. 14 The response of the vertical damper system to shock loading at various masses under zero pre-strain (**a**) and at various device pre-strains for a mass of 47 g (**b**)

3.4 Dynamical Modeling of One-Way Materials

For the linear bridge device made from the one-way material from Sect. 2.1, the FEM model developed in Sect. 2.4 was adapted, with the parameters given in Table 1. Contrary to the tensile pseudoelastic SMA, the transitions in the one-way material now include phase contributions x_α for all phases $\alpha \in \{M_+, M_-, A\}$ due to the heating to austenite and cooling down to a mixture of twinned martensite. Under normal operation, after cooling to room temperature the material will remain in the intermediate R-phase state, which is treated as a modified form of the common parent phase A

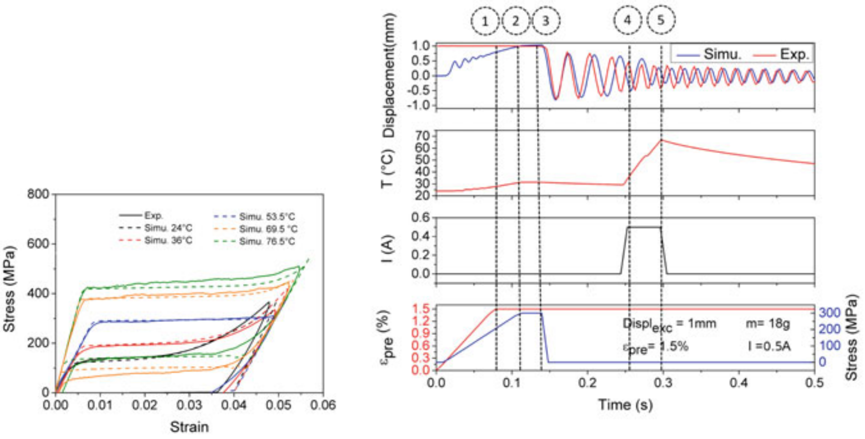

(a) (b)

Fig. 15 (**a**) Experiment (solid) and simulation (dashed): stress-strain response for one-way material; (**b**) Top panel: Simulation of proof mass displacement for a double bridge damper with active heat pulse (time steps 4–5), in comparison to experiment (red). Lower panels: temperature, heating current and pre-straining (ε_{pre}) to 1.5 % (steps 1–3)

(see Fig. 9a). This is accomplished by a transition path dependent latent heat (different for R→M, M→A or A→R transitions) and a temperature dependent elastic modulus

$$E_A(T) = E_R + \frac{1}{2}\left(1 + tanh\left(\frac{T - T'}{\Delta T'}\right)\right)(E_A - E_R),$$

where E_A and E_R are the moduli of A and R-phase (here, $E_M = E_R$), T' the approximate A-R transition temperature of 60 °C and $\Delta T'$ the transition interval of 5 °C. The pronounced hardening behavior apparent in the R-phase state is tackled by multiplying the plateau stresses with a hardening function $\sigma^{AM} = \sigma^{AM}(T)h(T, x_M)$, which depends on both temperature and martensite fraction. It is fitted to the tensile characterization data as $h(T, x_M) = 1 + \left(116.9 - 0.67T + 0.00955T^2\right) epx(\frac{x_M - 1}{0.15})$ and predicts well the tensile quasistatic loading in Fig. 15a. The simulation results for the mass displacement of a double bridge device under shock release is shown in Fig. 15b, where the initially ramped up load is held constant from time steps 2 to 3. In this experiment, a heating pulse (50 ms) is started delayed at point 4 in time to include the passive oscillation behavior. The increased amplitude reduction of the system is partly attributed to a stiffness increase, visible by a frequency increase from 29 to 59 Hz. From simulated stress and strain data, a specific damping capacity of 82 % is calculated for the first oscillation cycle after the pulse, which is nearly 50 % larger than for the same material in passive damping mode.

The dynamical simulations performed so far are based on a model originally developed for uniaxial loading. In case of film structure with higher structural complexity than simple bridges, a more complex strain path that depends on the loading history needs to be recorded. Furthermore, transitions between the low-temperature phase M and the metastable R-phase cannot always be excluded and simplified in the manner described above. To be able to numerically predict the associated response of three dimensional connected active/passive dampers, a phenomenological coupled multi-axial model for polycrystalline NiTi-based SMAs by Benešová et al. [12] and Sedlák et al. [13] is implemented in the ABAQUS finite element package within the user material subroutine UMAT for coupled temperature-deformation cycles. Based on the framework of continuum thermodynamics of irreversible processes, the model is capable of predicting dynamic loading including physical effects important in the multi-DoF SMA devices. Briefly, the model's features include: (i) a refined dissipation function coupling martensite transformation and reorientation processes, (ii) inclusion of the material responses associated with the transformation between austenite, martensite, and R-phase, (iii) the influence of tension-compression asymmetry; and the thermomechanical coupling, considering the strain-rate dependent latent heat generation/absorption during forward/reverse phase transformation where the localized martensite bands evolve. The following forms of free energy, dissipation function, and the heat equation are incorporated. The free energy is formulated as function of total strain $\varepsilon = e + \pi$ and inelastic strain π, martensite fraction ξ and temperature θ as

$$\begin{aligned}\Psi(\varepsilon(u), \pi, \xi, \theta) = \tfrac{1}{2} K\, tr(e)^2 + \mathscr{G}(\xi, \varepsilon) + \zeta(\pi, \xi) + \phi(\xi.\eta) + \delta_S(\pi, \xi)\\ + \tfrac{\nu}{2}|\nabla\pi|^2 + \tfrac{\nu}{2}|\nabla\xi|^2\end{aligned}$$

with ξ the martensite volume fraction, used to derive the driving force for transformation. The first two terms represent the elastic energy, $\zeta(\pi, \xi)$ a non-convex energy which, together with the last two gradient terms, is motivated by the localization of martensitic transformation, and $\phi(\xi, \eta)$ is the part of the chemical energy driving the thermomechanical coupling [12]. The dissipation function comprises the rate-independent part r_{RI} which depends on the transformation direction ($\dot{\xi}$), while the term r_{VI} denotes the viscous contribution [12]:

$$\begin{aligned}\mathscr{R}_{TOT} &= r_{RI}(\pi, \xi, \theta, \dot{\pi}, \dot{\xi}) + r_{VI}(\dot{\pi}, \dot{\xi}) \quad \text{with}\\ r_{RI}(\pi, \xi, \theta, \dot{\pi}, \dot{\xi}) &= \begin{cases} a_{reo}(\theta)|\dot{\pi}| + a_{AM}(\xi)\dot{\xi}, & \text{if } \dot{\xi} \geq 0\\ a_{reo}(\theta)(|\pi\dot{\xi}/\xi| + |\dot{\pi} - \pi\dot{\xi}/\xi|) + a_{MA}(\xi)\dot{\xi}, & \text{if } \dot{\xi} < 0\end{cases}\\ r_{VI}(\dot{\pi}, \dot{\xi}) &= \tfrac{\mu}{2}|\dot{\pi}|^2 + \tfrac{\mu}{2}|\dot{\xi}|^2\end{aligned}$$

By solving the heat equation

$$\dot{\omega} - div(\mathbb{K}(\xi, \theta)\nabla\theta) = r_{RI}(\pi, \xi, \theta, \dot{\pi}, \dot{\xi}) + 2r_{VI}(\dot{\pi}, \dot{\xi}) + \dot{\xi}\partial_{\xi}\phi(\xi.\eta)$$

the model can reproduce localized transformation at different strain rates related to heat transfer effects. This kind of approach is a prerequisite to the simulation of complex SMA structures in Sect. 4.2.

4 Two-DoF Vibration Stabilization Platform

The phase transformation between martensite and austenite for one-way SMA generates large recovery force allowing for active vibration control. The operating frequency of SMA actuator is limited by the cooling down time of the actuator. Therefore, a miniaturized SMA actuator is favourable for low frequency vibration control application below 100 Hz, owing to reduced power consumption for device heating and faster cooling. A prospective application is to compensate against the vibrations introduced by hand movement in smartphone camera where the typical operating frequency is below 10 Hz. In contrast to the vibration control using voice coil motor, less components are required for SMA based stabilizers facilitating miniaturization. The authors present a 2-DoF vibration stabilization platform for smartphone cameras to compensate for the vibrations arising from hand movements. The design criteria is to stabilize rotational movements of 1° along x and y axis based on the desirable specifications for Optical Image Stabilization (OIS) system [11].

4.1 Construction and Operation

A monolithic SMA device design is adopted for the stabilization platform to enable ease of assembly as shown in Fig. 16a. Using a NiTi foil of 15 μm thickness, four SMA actuators of bridge structure having a width of 65 μm are micromachined by laser cutting. A short current pulse of 0.2 A for 20 ms is used to raise the bridge temperature to 80 °C. After removal of heating pulse, the bridge requires 55 ms to reach the starting state (Fig. 16b), achieving a maximum operating frequency of 13 Hz.

The construction of the OIS system is illustrated in Fig. 17a and the assembled device (without top cover) is shown in Fig. 17b.

Figure 18 shows the operation of the OIS system. A short heating pulse of 20 ms is used to enable phase transformation to austenite. The antagonistic bridge pair SMA_1 and SMA_3 are activated sequentially to estimate the maximum tilting angle. The displacement is traced using laser displacement sensor on SMA_1. A maximum displacement of 65 μm is achieved, corresponding to a tilting angle of 1°.

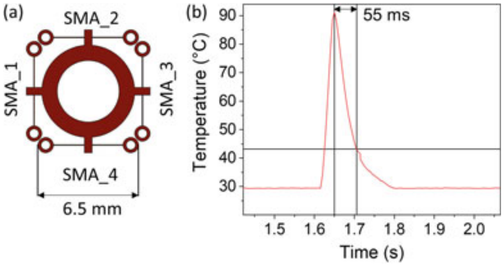

Fig. 16 (**a**) Monolithic SMA design for 2-DoF vibration stabilization and (**b**) its thermal response on a short heating pulse of 20 ms. The device cools down to the starting state in 55 ms

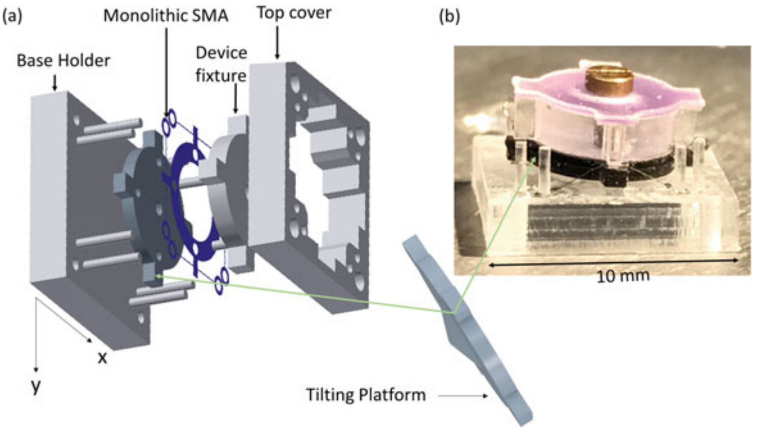

Fig. 17 The exploded view, illustrating the assembly of 2-DoF vibration stabilization platform (**a**) and the system after assembly (without top cover) (**b**)

Fig. 18 The stabilization angle of 1° is achieved in this system by sequential activation of antagonistic pairs SMA_1 and SMA_3

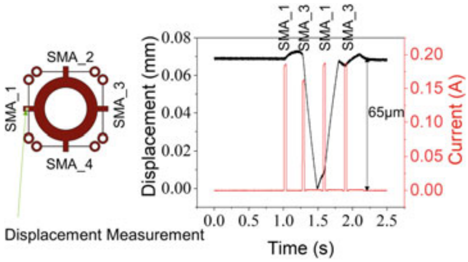

4.2 Static Simulation of the Two-DoF Vibration Stabilization Platform

The implemented multi-axial model is applied for an analysis of the stress-strain-phase transformation evolution upon single pulse heating. After the device has been pre-strained (Fig. 19a) the SMA_1 element is heated, where temperature changes homogeneously in the activated material and tilting to the observed angle follows. This leads to a coupled deformation of the opposed SMA_3 across the device. Figure 19b shows the total strain in the structure. The tilting, which occurs due to transformation-strain recovery in SMA_1 upon heating, results in additional progress of transformation in SMA_3. This leads to the actuation of SMA_1 under a variable bias triggered from SMA_3 (actuation under variable stress as in [14]). Figure 20a represents the related stress-temperature evolutions for SMA_1 and SMA_3 accompanied by the material's characteristic Clausius-Clapeyron transformation lines (blue lines for A→M, green lines for M→A phase transition), and in Fig. 20b the correlated stress-strain responses are shown simultaneously. The resulting coupling gives rise to the observed overshoot of the tilt actuator displacement during actuation in Fig. 18 (right).

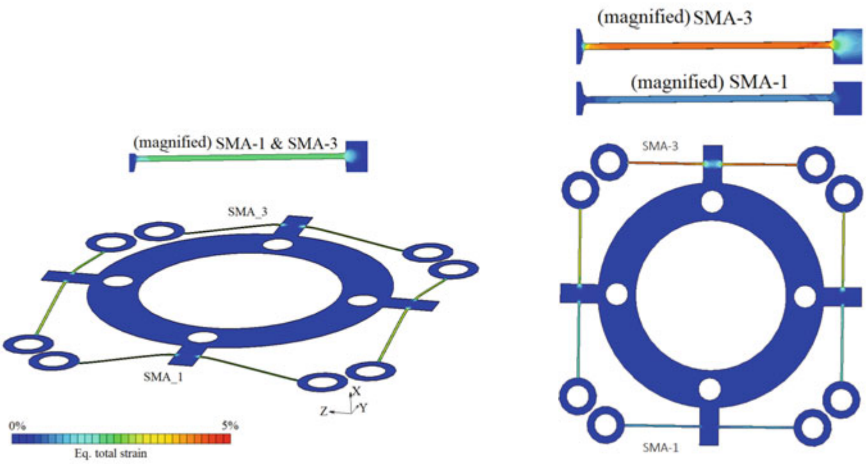

(a) (b)

Fig. 19 Induced equivalent total strain after pre-straining of the device (**a**) and after actuation of bridge SMA_1, which causes tilting (**b**, top view)

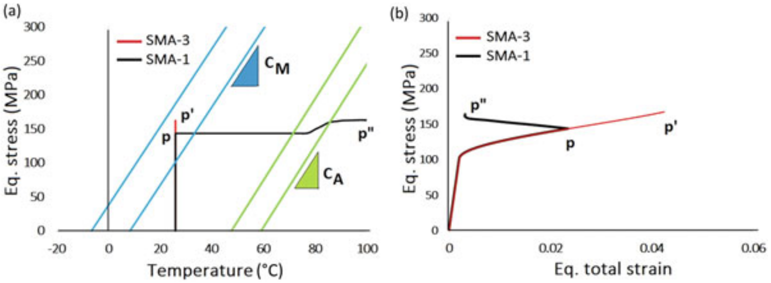

Fig. 20 Stress-temperature paths for two opposed bridges SMA_1 and SMA_3 from Fig. 19b, state after pre-straining for both SMAs: Point P, after heating: P’ for SMA_3, P” for SMA_1 (**a**); The coupled stress-strain behavior in the SMAs (**b**). The blue and green lines represent the forward and reverse transformation stresses, their inclination is given by the Clausius-Clapeyron coefficients C_M and C_A

5 Conclusions

The energy dissipation of thin film/foil SMA materials mostly depends on loading strain, pre-strain and loading rate. Pre-strain and loading strain are crucial design parameters to maximize energy dissipation. In pseudoelastic SMA, pre-straining close to the beginning of transformation plateau results in achieving repeatable energy dissipation behaviour in all loading cycles. From a uniaxial tensile loading of the material, up to 34 % of loading energy is dissipated for the pseudoelastic SMA and 86 % for the one-way SMA material. In a damper system containing double bridge device, high SDCs of 70 and 90 % are achieved using pseudoelastic and one-way SMA devices, respectively. Short current pulses below 100 ms enable more homogenized temperature distribution on one-way device achieving better phase transformation. For vertical shock loading with guided mass movement, the mass stabilizes without any oscillation after shock loading, showing large application potential as shock absorber in miniature robotics. For the dynamic simulation of bridge actuators, FEM models for 2D plane stress simulations of the bridge domains are combined with a thermally activated kinetic reaction model for phase transformations. For pseudoelastic and one-way SMAs, this approach well predicts the transient response, where localization of transformation and the accumulation of martensite phase in the SMA explain limitations of the damping capacity.

Miniaturized SMA actuators for 2-DoF tilt stabilization have demonstrated an operating frequency range up to 13 Hz. Ease of assembly is achieved using a monolithic device design. The more complex kinematics requires the use of multi-axial constitutive models with thermomechanical coupling to allow a precise prediction of the interference of strain and temperature across the distributed active SMA parts.

Acknowledgements The authors gratefully acknowledge funding by the German Science Foundation (DFG) within the priority program SPP1897. The authors appreciate the support of Nicholas Case in conducting single-bridge experiments.

References

1. Dixon, J.C.: The Shock Absorber Handbook. John Wiley & Sons (2008)
2. Wilson, S.A., Jourdain, R.P., Zhang, Q., Dorey, R.A., Bowen, C.R., Willander, M., Wahab, Q.U., Al-hilli, S.M., Nur, O., Quandt, E., Johansson, C.: New materials for micro-scale sensors and actuators: an engineering review. Mater. Sci. Eng. R: Rep. **56**(1–6), 1–129 (2007)
3. Jacob, K., Ahmadi, S., Wendler, F., Miyazaki, S., Gueltig, M., Kohl, M.: Shape memory foil-based active micro damping for portable applications. In: Transducers Conference, Berlin, Germany, vol. 23, pp. 590–593 (2019). (Jun 2019)
4. Müller, I., Seelecke, S.: Thermodynamic aspects of shape memory alloys. Math. Comput. Model. **34**, 1307–1355 (2001)
5. Wendler, F., Ossmer, H., Chluba, C., Quandt, E., Kohl, M.: Mesoscale simulation of elastocaloric cooling in SMA films. Acta Mater. **136**, 105–117 (2017)
6. Ahmadi, S., Jacob, K., Wendler, F., Padhy, A., Kohl, M.: Active damping of thin film shape memory alloy devices. Proc. Appl. Math. Mech. **20**, 202000310 (2020)
7. Ahmadi, S., Jacob, K., Wendler, F., Kohl, M.: Shape memory alloy film damping for smart miniature systems. Int. J. Smart Nano Mater. **9**(3), 199–215 (2018)
8. Ahmadi, S., Jacob, K., Wendler, F., Kohl, M.: Mesoscale simulation of shape memory alloy film damping. Proc. Appl. Math. Mech. **18**, 201800409 (2018)
9. Jacob, K., Sessner, V., Miyazaki, S., Kohl, M.: Active vibration damping and control using SMA foil-based devices. In: ACTUATOR 2021, pp. 200–203 (2021). ISBN 978-3-8007-5454-0
10. Jacob, K., Case, N., Miyazaki, S., Kohl, M.: Miniature shock absorber based on SMA foil actuation. In: ACTUATOR 2022 pp. 330–333 (2022). ISBN 978-3-8007-5894-4
11. La Rosa, F., Virzì, M.C., Bonaccorso, F., Branciforte, M.: STMicroelectronics. Optical image stabilization (2015). http://www.st.com/resource/en/white_paper/ois_white_paper.pdf. Accessed 14 Feb 2022

12. Benešová, B., Frost, M., Kadeávek, L., Roubíek, T., Sedlák, P.: An experimentally-fitted thermodynamical constitutive model for polycrystalline shape memory alloys. In: Discrete and Continuous Dynamical Systems Series S, vol. 14, pp. 3925–3952 (2021)
13. Sedlák, P., Frost, M., Benešová, B., Ben Zineb, T., Šittner, P.: Thermomechanical model for NiTi-based shape memory alloys including R-phase and material anisotropy under multi-axial loadings. Int. J. Plast. **39**, 132–151 (2012)
14. Shayanfard, P., Heller, L., Šandera, P., Šittner, P.: Numerical analysis of NiTi actuators with stress risers: the role of bias load and actuation temperature. Eng. Fract. Mech. **244**, 107551 (2021)